Eur Biophys J (1990) 19:11–18

European Biophysics Journal

The photocycle and the structure of iron containing bacteriorhodopsin – a kinetic and Mössbauer spectroscopy investigation

M. Engelhard [1], K. D. Kohl [1]*, K. H. Müller [1], B. Hess [1], J. Heidemeier [2], M. Fischer [2], and F. Parak [2]

[1] Max-Planck-Institut für Ernährungsphysiologie, Rheinlanddamm 201, D-4600 Dortmund, Federal Republic of Germany
[2] Molekulare Biophysik, Fachbereich Biologie, Universität Mainz, Welder-Weg 26, D-6500 Mainz, Federal Republic of Germany

Received February 9, 1990/Accepted in revised form June 20, 1990

Abstract. Bacteriorhodopsin (bR), converted by deionization to the blue form was reconstituted to the active purple membrane by the addition of Fe^{2+} or Fe^{3+} ions. ^{57}Fe Mössbauer spectra of these samples were measured at different pH values (pH 3.9, pH 5.0 and pH 7.0) and at temperatures ranging from 4 K to 300 K. The hyperfine parameters reveal two iron environments with oxygen atoms in the neighbourhood of iron. Iron type 1 is in the 3^+ high spin state. It is bound to acid side chains of the protein and/or the phosphate groups of the lipids. Iron type 2 is in the 2^+ high spin state and is linked to carboxy groups of the protein in a rather unspecific way. Dynamics as measured by Mössbauer spectroscopy show that the purple membrane becomes flexible only above 220 K. At the interface between membrane and bulk water the mobility is comparable to that of proteins with hydrophilic surfaces. The photocycle of Fe^{3+}-bR is slowed down compared to native bR. 3–5 Fe^{3+}/bR are sufficient to inhibit the photocycle turnover by one order of magnitude. This specific effect is also found with Cr^{3+}, though it is less pronounced. Mössbauer spectra of Fe^{3+}-bR at 4 K reveal that iron nuclei are spin-coupled, indicating their close spatial proximity. It is proposed that iron trinuclear clusters interact with the proton uptake site of bR.

Key words: Bacteriorhodopsin – Mössbauer spectroscopy – Cation binding site

Introduction

Bacteriorhodopsin (bR), the light driven proton pump from Halobacterium halobium (Oesterhelt and Stoeckenius 1971; for recent reviews see Ovchinnikov et al. 1982; Stoeckenius and Bogomolni 1982; Oesterhelt and Tittor 1989), can be converted into a blue species either by acidification (Fischer and Oesterhelt 1979; Mowery et al. 1979; Edgerton et al. 1980; Kobayashi et al. 1983) or by deionisation (Kimura et al. 1984; Chang et al. 1985). On light-excitation of acid- or the cation depleted "blue membrane" a photocycle is observed which has, however, no resemblance to the one of the native bR. The M-intermediate, which is characterized by an unprotonated Schiff base is not present (Kobayashi et al. 1983; Chang et al. 1985, Chronister et al. 1986; Ohtani et al. 1986; Váró and Lanyi 1989). Furthermore, the blue membrane does not pump protons (Drachev et al. 1978; Dèr et al. 1989). The purple colour can be restored on the addition of cations (Kimura et al. 1984; Chang et al. 1985; Ariki and Lanyi 1986; Zubov et al. 1986). In the native membrane one Ca^{2+} and five Mg^{2+} are bound (Chang et al. 1985; Ariki and Lanyi 1986) suggesting a specific requirement for these cations. However, in reconstitution experiments with a wide variety of metal ions no specificity of cation binding could be demonstrated.

It is now well established that cations are not directly involved in the colour regulation of purple membrane. The colour transition is solely determined by the surface pH which influences conformational states of the protein (Szundi and Stoeckenius 1987, 1989). However, these data do not contradict the assumption that specific cation binding sites of functional and/or structural importance may exist.

It was proposed from binding studies that there are a couple of high and low affinity sites present either on the lipid part or on the protein part (Ariki and Lanyi 1986; Duñach et al. 1987, 1988). In other studies cation binding sites were further analysed (Engelhard et al. 1987). Katre et al. (1986) determined cation binding sites by X-ray diffraction studies. Corcoran et al. (1987) deduced from their data that there were three different cation environments. Two of the sites are located on the surface with three and six water molecules as ligands. The third site might be in a more hydrophobic region. Sequence studies, as well as solid state NMR experiments, point to at least one distinct cation binding site located on the cytoplasmic surface

* *Present address:* Bayer AG, Analytisches Labor, D-5600 Wuppertal-Elberfeld, Federal Republic of Germany
Offprint requests to: M. Engelhard

which comprises the loop between helices C and D and is in the proximity of helix G (Engelhard et al. 1989a, b).

In contrast to all mono- and divalent cations so far tested, certain trivalent ions slow down the photocycle turnover (Drachev et al. 1984; Duñach et al. 1987; Chang et al. 1986). Especially, La^{3+}-ions were found to inhibit the second half of the photocycle. Another ion which similarly affects the function is Fe^{3+}.

The present report describes the functional properties of bacteriorhodopsin with incorporated ^{57}Fe and Mössbauer experiments on the dark adapted state. This specific cation provides the opportunity to gain information about the nature of iron binding sites using Mössbauer spectroscopy. This technique also allows one to study dynamic properties of the purple membrane.

Material and methods

Materials

All reagents used were reagent grade. Bacteriorhodopsin was isolated from Halobacterium halobium using the method of Oesterhelt and Stoeckenius (1974). The blue membrane was prepared according to Kimura et al. (1984). The purple chromophore was regenerated by adding appropriate amounts of cations and raising the pH to 6 by the addition of diazabicyclundecene (DBU) as a bulky organic base. This base was chosen because the corresponding protonated cation (DBU * HCl) can only convert the blue membrane into the purple form by using a thousand fold molar excess of the reagent. Flash photolytic experiments were performed with a laser flash from a YAG-Laser (Quantel, Paris) (10 ns, 570 nm).

Preparation of Fe-bR

The iron-bacteriorhodopsin was obtained by titrating the blue membrane with $^{57}Fe^{2+}$ or $^{57}Fe^{3+}$. The samples were washed with water by centrifugation. The pH of the membrane suspension was adjusted to the desired value by adding either 30% diazabicycloundecene (DBU) in water or HCl. Mercaptoethanol was added to stabilize Fe^{2+}. It was, however, not possible to obtain pure ferrous bR. Wet samples were obtained either by centrifugation or by freeze-drying the pellet and subsequently adding water to obtain a wet paste. The amount of iron was determined by atomic absorption spectroscopy. A number of samples which differed in the Fe content, the pH, and the water content were used for Mössbauer spectroscopy. Table 1 summarizes the preparations.

Analysis of the photocycle

The photocycle was measured at six different wavelength (415 nm, 500 nm, 570 nm, 600 nm, 620 nm und 650 nm) over a time range of 10^7 µs using four overlapping time intervals. The whole set of data were analysed using a method comparable to that of Nagle et al. (1982) or Maurer et al. (1987) with some additional statistical properties. The data errors are estimated from the data trace preceeding the signal. This information is used to estimate the data weights. The error standard deviation has an expected value of 1/ln 10 in estimation units. The errors standard deviation computed from the residuals of the fit is a test of whether a further exponential term is required or not. Details will be published elsewhere.

Table 1. Bacteriorhodopsin samples used for Mössbauer spectroscopy

Sample	Fe/bR	Oxidation state	H_2O(mg)/ 60 mg bR	pH
1	0.6	2+, 3+	80	3.9
2	0.6	2+, 3+	100	5
3	3.15	2+, 3+	>100	7
4[a]	3.15	2+, 3+	dry	–
5	5	3+	100	5

[a] Sample 4 originated from sample 3 by lyophilization

Mössbauer spectroscopy

Mössbauer spectra of ^{57}Fe-bR (60 mg) were measured between 77 K and 250 K. In some cases measurements at lower temperatures (4.2 K, 10 K, and 18 K) were performed. The temperature was stabilized to better than 2 K. A conventional Mössbauer spectrometer with sinusoidal velocity profile was used (For details see Parak and Reinisch 1986).

Results

Photocycle of cation-reconstituted bR

The binding of ferrous and ferric ions to the blue membrane with apparent dissociation costants of $Kd = 10^{-6}$ and $Kd = 10^{-7}$, respectively, are comparable to other di- and trivalent cations (e.g. Ariki and Lanyi 1986; Engelhard et al. 1989b).

After flash excitation of an iron containing sample (5 Fe^{3+}/bR) the absorbance changes at 415 nm and 570 nm were recorded. They are, together with the corresponding traces of native bR, represented in Fig. 1. It should be noted that the time scale is logarithmic with the range from µs to 10 s. Whereas in native bR the turnover is approximately 30 ms, the Fe^{3+}-bR sample needs almost one second to reach the original ground state. The formation of M^{412}, the long lived intermediate of the bR photocycle, is nearly identical for both samples. However, the decay-rates differ markedly. Fe^{3+}-bR stays for one to two order of magnitudes in the M-state before relaxing back to the bR ground state. In native bR the M^{412} almost immediately decays to its original bR^{570}-state.

To elucidate further the influence of trivalent ions on the photocycle of bR it was analysed using the absorbance changes at six different wavelength (415 nm, 500 nm, 570 nm, 600 nm, 620 nm, and 650 nm). The best

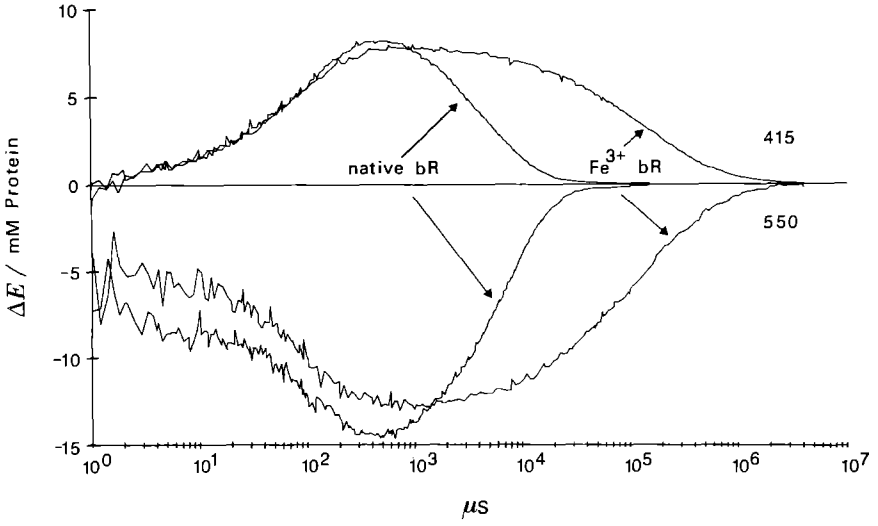

Fig. 1. Absorbance changes at 415 nm and 570 nm after excitation of native bR and Fe^{3+}-bR by a laser pulse (10 ns, λ_{max}, 570 nm). The pH was adjusted to pH 6 with DBU

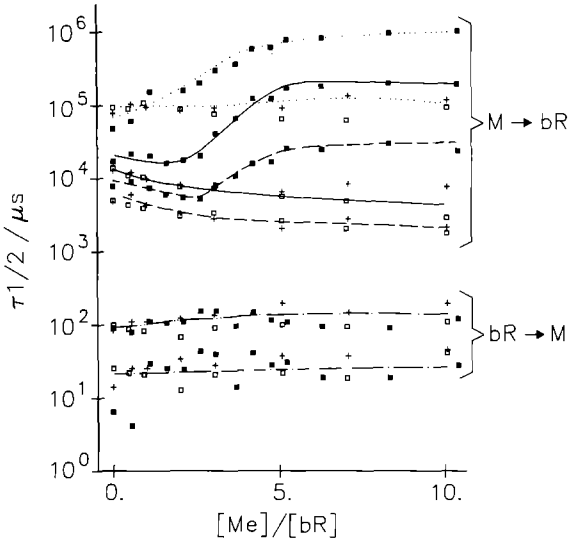

Fig. 2. Kinetic constants of the photocycle of action reconstituted bR. The pH of the samples were adjusted to pH 6 with DBU. The photocycle was fitted with a sum of five exponentials. The corresponding half-life times are plotted against the cation content of the bR-samples. **a** Fe^{3+}-bR ■■■ **b** Mg^{2+}-bR □□□ **c** La^{3+}-bR + + +. The connecting lines were drawn to aid the eye (τ_1: - · - · - · - τ_2: · · · · · · · · · · · · τ_3: - - - - - τ_4: ——— τ_5: · · · · ·)

approximation to the experimental data was obtained with a sum of five exponentials with half-life times $\tau_1 - \tau_5$. This holds for all preparations. The first two exponentials with τ_1 and τ_2 between 10 μs and 100 μs are associated with the formation of *M*, whereas the other three components τ_3 to τ_5 describe the second part of the photocycle. Figure 2 shows these kinetic parameters plotted against the cation content of the sample. Mg^{2+} was chosen as a representative example for divalent ions. For La^{3+} containing bR an effect on photocycle and proton pump has already been demonstrated for higher La^{3+} concentrations (Drachev et al. 1984; Chang et al. 1985; Ariki et al. 1987; Duñach et al. 1987). Whereas Mg^{2+} and La^{3+} have no influence on the photocycle in the concentration range measured, the Fe^{3+} ion slows down the photocycle turnover by one order of magnitude if the concentration exceeds $2\,Fe^{3+}$/bR. The maximal retardation is obtained at an iron content of about $5Fe^{3+}$/bR. Other cations tested such as Fe^{2+}, Pr^{3+}, Eu^{3+}, and Yb^{3+} do not show this pronounced effect. An exception was found in Cr^{3+} which inhibits the photocycle in a similar fashion to Fe^{3+} but only by a factor of 0.5.

It should be noted that the first data points of these analyses stem from samples without added cations. The pH was raised to pH 6 by the organic base DBU in order to re-establish the purple form of bR. Furthermore, the photocycle kinetics are similar if not identical to samples with a higher content of cations and to untreated purple membrane (see for example the data of Mg-bR, Fig. 2). The corresponding protonated base, as already mentioned above, is not able to provoke the blue-purple transition in this concentration range (data not shown), indicating – in agreement with Szundi and Stoeckenius (1987, 1989) – that the surface pH is responsible for the formation of the purple colour.

Mössbauer spectra of ^{57}Fe-bR

A Mössbauer spectrum of ^{57}Fe substituted bR as representative example is shown in Fig. 3. The experimental data of the different bR samples (Table 1) can be fitted by two quadrupole doublets with the quadrupole splittings QS_1 and QS_2. QS_1 varies between 0.32 and 0.80 mm/s, whereas the isomer shift, IS_1, is about 0.5 mm/s (Fe type 1). Low temperature spectra at 10 K or 18 K showed a substantial decrease of the absorption area and a rather poorly resolved magnetic hyperfine pattern. These facts suggest that the type 1 iron is in the 3^+ high spin state. The second doublet shows a splitting, QS_2 of the order of 3 mm/s and an isomer shift, IS_2, of about 1.38 mm/s (Fe type 2). While QS_2 has a strong temperature dependence (compare Fig. 4) the isomer shift varies only slightly with temperature. The hyperfine parameters prove that the type 2 iron is in the 2^+ high spin state. A close inspection of Fig. 3 indicates that QS_2 comes from the nearly unre-

Table 2. Hyperfine parameters obtained from a least squares fit of Lorentzians to the Mössbauer spectra at 80 K. Fits with two (QS_1; QS_2) or three (QS_1 to QS_3) doublets. For samples 1 and 2 the spectra measured between 80 K and 250 K were used to perform a linear extrapolation of IS_1 and IS_2 to 300 K

Sample No.	IS_1 [mm/s]		QS_1 [mm/s]	IS_2 [mm/s]		QS_2 [mm/s]	IS_3 [mm/s]	QS_3 [mm/s]
	80 K	300 K	80 K	80 K	300 K	80 K	80 K	80 K
1	0.47	0.45	0.42	1.39	1.21	3.24		
				1.40		3.34	1.40	2.90
2	0.52	0.45	0.52	1.47	1.26	3.26		
3	0.53		0.62	1.38		3.24		
4	0.52		0.68	1.38		2.95		
				1.35		3.19	1.35	2.46
5	0.53		0.61					

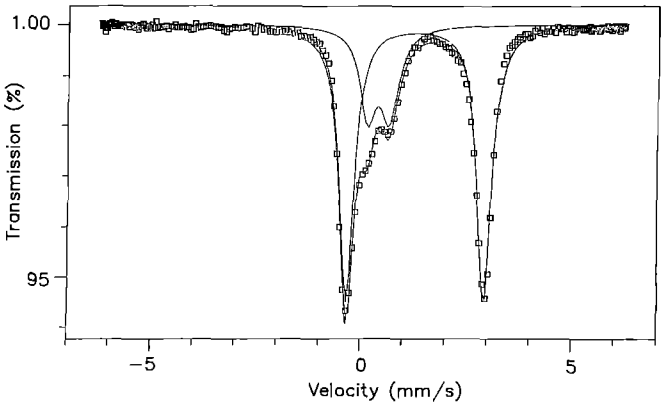

Fig. 3. Typical Mössbauer spectrum of ^{57}Fe in bR. The spectrum was taken from sample 2 at 80 K. Solid lines give a least squares fit of two quadrupole doublets to the experimental data

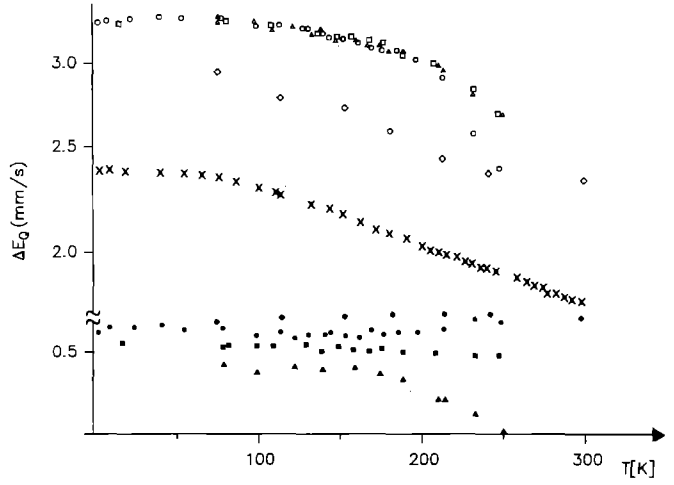

Fig. 4. Temperature dependence of the quadrupole splitting. Full symbols: iron type 1, open symbols: iron type 2; triangles, sample 1; squares: sample 2; circles: sample 3; diamonds: sample 4, freeze dried sample 7

solved quadrupole doublets which represent two iron postitions with slightly different environments. This is taken into account in the fits for samples 1 and 4 (see Table 2).

Table 2 gives the fit parameters of spectra taken at 80 K. Two alternatives are given for sample No. 1 and 4.

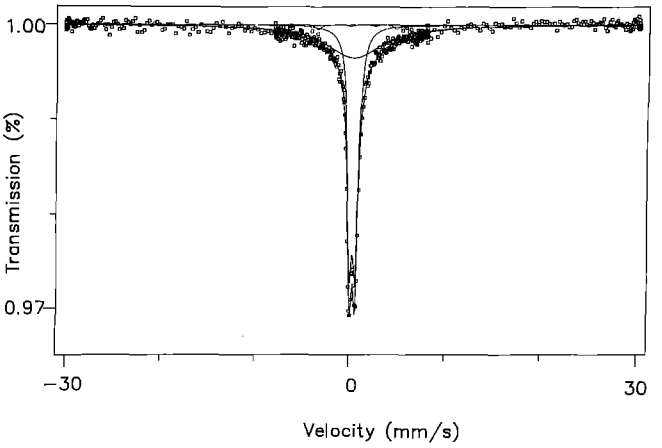

Fig. 5. High velocity Mössbauer spectrum of sample 2 at 235 K. The spectrum contains two separate measurements with maximal velocities of 8 and 30 mm/s, respectively. They were normalized by a spline fit procedure to each other

In the first only one large quadrupole doublet QS_2 was assumed while in a second fit two large doublets with QS_2 and QS_3 were allowed. Here, IS_3 was fixed to the value of IS_2. The isomer shifts, IS_1 and IS_2, at 300 K are determined by linear regression of values measured between 80 K and 250 K to allow a comparison with results from the literature.

As can be seen from Table 2 the quadrupole splitting QS_1 depends on the pH value of the bR-sample and in creases with increasing pH. The differences in the QS_1 values become even more pronounced when comparing the temperature dependence. For the pH 3.9 sample the splitting vanishes at 250 K. Changing the pH alters the geometry of the ligands around the Fe^{3+} binding site. It is remarkable that this effect is most pronounced for the blue membrane (sample 1) which differs strongly from the native purple membrane.

Temperature dependence of the quadrupole splitting

Figure 4 gives the temperature dependence of the quadrupole splittings. Below 200 K the splitting QS_2 (Fe^{2+}) is the same for all hydrated bR samples (No. 1, 2 and 3). The temperature dependence is the typical one. For Fe^{2+} bound to myoglobin the decrease of QS_2 is nearly linear

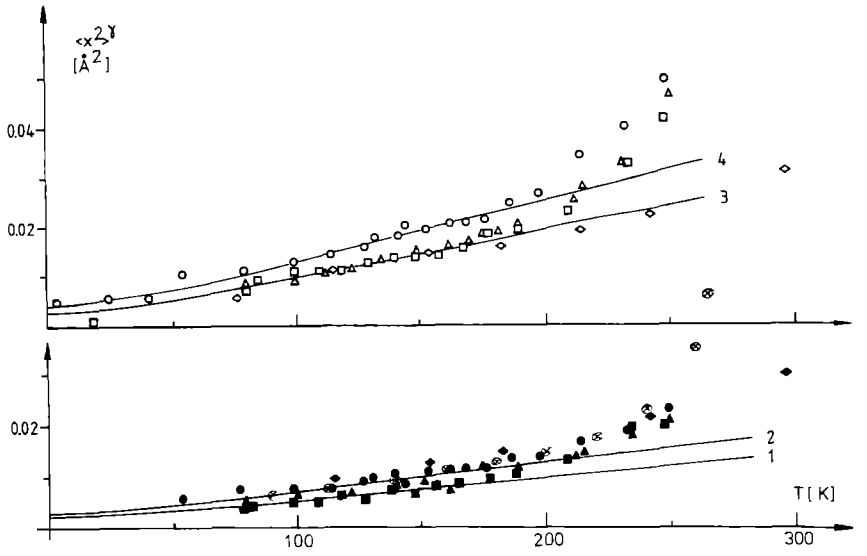

Fig. 6. Mean square displacements ($\langle x^2 \rangle$) of iron in bR-sample as function of temperature. Full symbols: iron type 1; open symbols: iron type 2; triangles: sample 1; squares: sample 2; circles: sample 3; diamonds: freeze dried sample 4; open circles with crosses: remeasurement of sample 3 after complete oxidation of Fe^{2+} to Fe^{3+}. Solid lines 1 to 4: Debye law with the Debye temperature $\theta_D = 230$ K, 200 K, 165 K, and 145 K, respectively

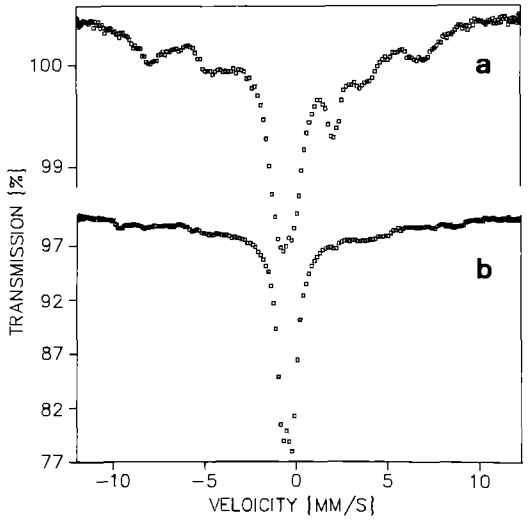

Fig. 7a, b. Mössbauer spectra of Fe^{3+}-bR at $T = 4.2$ K. **a** sample 2 with 0.6 Fe^{3+}/bR; **b** sample 5 with 5 Fe^{3+}/bR

between 100 K and 300 K (Parak et al. 1981). In the bR-samples, however, a stronger decrease of QS_2 with T occurs above 200 K. This feature is most significant in sample No. 3 which contains the largest amount of water.

At a particular temperature below 200 K the ratio of the absorption areas of Fe^{3+} and Fe^{2+} depends on the preparation and on the time the sample is kept at room temperature before freezing. In samples kept at 240 K the Fe^{2+} oxidizes after some weeks to Fe^{3+}. Addition of small amounts of mercaptoethanol stabilizes the Fe^{2+} for a longer time.

Temperature dependence of the mean square displacement $\langle x^2 \rangle$

The temperature dependence of the absorption area of a Mössbauer spectrum yields the mobility of the iron as determined by its environment. From the Lamb Mössbauer factor, f, the dynamic mean square displacement, $\langle x^2 \rangle$, of the iron can be obtained. Details of the data analysis are given by Parak and Reinisch (1986).

In protein samples, additional broad absorption lines were found (compare for instance Parak et al. (1982)) indicating diffusive motions in limited space with a characteristic time between 1 and 100 ns. These lines have to be separated from the narrow Mössbauer lines in the calculation of $\langle x^2 \rangle$-values. In the bR samples these lines are difficult to resolve at temperatures lower 240 K and do not contribute significantly to the area of the narrow lines. However, the spectrum at $T = 260$ K shown in Fig. 5 proves that, in bR at higher temperatures, quasi-diffusive motions are also present.

Results of the mean square displacement $\langle x^2 \rangle$, of the Fe in different samples are shown in Fig. 6. It should be mentioned that the absolute values of $\langle x^2 \rangle$ were obtained by a normalisation procedure assuming a linear temperature dependence of $\langle x^2 \rangle$ well below 200 K and the value $\langle x^2 \rangle = 0$ at $T = 0$ K. As shown in Fig. 6 the $\langle x^2 \rangle$-value of Fe^{2+} increases more than proportionally with temperature above 200 K. This feature is also found for Fe^{3+}. Note, that the slope of $\langle x^2 \rangle$ versus T is much smaller in case of Fe^{3+} below 200 K. Drying the sample reduces the increase of $\langle x^2 \rangle$ above $T = 200$ K.

Hyperfine structure of Fe^{3+} *bR*

As already mentioned the Fe^{3+} spectrum shows a rather diffuse magnetic hyperfine splitting at 4.2 K (Fig. 7a). This diffuse pattern is reduced on increasing the iron content of the sample (sample 5) (Fig. 7b). This can be interpreted by postulating that at larger Fe^{3+}/bR stoichiometries a spin-spin coupling of the iron atoms occurs, indicating their close spatial contact.

Discussion

In the following section the environment of the iron cations as reflected by the hyperfine parameters and the temperature dependency of the Mössbauer parameter

will be discussed. These data provide not only an insight into the dynamic and structural properties of the Fe-bR samples but also allow an explanation for the impairment of the function of Fe^{3+}-bR.

Properties of the iron-environment

For the clarity of the following discussion possible features of the binding of cations to the purple membrane should be defined. Generally there are two possibilities for cations to interact with a membrane protein such as bacteriorhodopsin: The cations may be smeared out on the interface between membrane and bulk water without well defined ligands (unspecific site) or they may be bound to specific sites which can be lipid and/or protein binding sites (specific site). These latter sites may have different affinities.

An estimation of the stability of carboxyl- and phosphate-iron complexes (Bjerrum et al. 1958) reveals that the Fe^{3+} samples are generally more stable than the Fe^{2+}-complexes. Fe^{2+} and Fe^{3+} complexes of monovalent carboxylic acids such as formic- or acetic acid are not formed in water. However, oxalic acid forms stable complexes with Fe^{2+} and Fe^{3+} in the whole pH range under investigation. Fe^{3+}-phosphate complexes are not hydrolyzed in water whereas the corresponding Fe^{2+}-compounds are unstable. Taking these data into account one would expect Fe^{3+} to bind to purple membrane at specific sites, if phosphate groups and/or more than one carboxylic side chain are available. On the other hand, Fe^{2+}-cations are likely to be attached only electrostatically to the surface of the purple membrane.

The quadrupole splittings of the Fe^{2+}-atoms are reduced considerably at temperatures above 200 K (Fig. 4). This observation can be correlated with the mobility of surface bound water. It is well known that water bound to surfaces has a viscosity as high as ice below 200 K, while the viscosity strongly decreases above 200 K (e. g. Parak et al. 1982; Singh et al. 1981). If the iron is exposed to the water the field gradient is averaged more and more with increasing water mobility and in this way reduces the quadrupole splitting (see Fig. 4). The mechanism is similar to the well known motional narrowing in NMR. The $\langle x^2 \rangle$-values of Fe^{2+} also increase more than linearly with temperature above 200 K (see Fig. 6). All these features can be understood with the assumption that Fe^{2+} is only very loosely bound and does not form a stable complex. A stronger binding to the membrane only occurs if water is removed, yielding a reduction of QS_2 as already mentioned and a decrease of the $\langle x^2 \rangle$-values above 200 K. From these data, it can be concluded that Fe^{2+} binds non-specifically and labels, therefore, mainly the interface between the membrane and bulk water.

In contrast to these findings, Fe^{3+}-cations are marking the properties of the biological membrane. The high binding constants of Fe^{3+} to phosphate or carboxyl groups make binding-sites very probable. This is also reflected in the mean square displacements. Below 200 K, $\langle x^2 \rangle$-values increase only modestly with temperature. The linear increase can be described by a Debye model. This allows one to characterize the vibrational behaviour with only one parameter, the Debye temperature θ_D, although it is well known that a protein does not fulfil the conditions for which the Debye law applies. For Fe^{3+}-bR, θ_D is between 230 and 200 K. As already mentioned, the viscosity of surface bound water decreases drastically above 200 K and this usually increases the protein flexibility (Singh et al. 1981; Parak et al. 1982). Since the additional increase of the $\langle x^2 \rangle$-values between 200 K and 230 K is rather small we can conclude that the flexibility of the system at the Fe^{3+} site is not strongly correlated with the water mobility. A strong increase of the $\langle x^2 \rangle$-values, which is absent in dry samples, does, however, occur at higher temperatures. Apparently, the temperature has to be considerably above the glass transition so that the lower water viscosity allows the membrane system to fluctuate.

In contrast to the isomer shift the quadrupole splitting QS differs significantly for most of the samples (Table 2). This allows conclusions about the symmetry of the iron complex. In general, the QS is determined by two parts of the electric field gradient. First, an asymmetry of the 3d electrons gives the contribution q_{val}. Another part, q_{lat}, arises from all surrounding ions. Both contributions are modified by the Sternheimer factors $(1-R)$ and $(1-\gamma^{\infty})$, respectively (Sternheimer 1963). Direct lattice sum calculations of Nozik and Kaplan (1967) have shown that q_{lat} vanishes for an iron hexaquo complex. The ground state of Fe^{3+} is an S-state. Neglecting mixing with higher states q_{val} also vanishes, which means $QS_1 = 0$ (Nozik and Kaplan 1968). Therefore, bR samples contain no pure Fe^{3+}-(H_2O)-complexes; carboxyl groups and/or phosphate groups take part in the coordination of the iron as expected from the binding constants (Ariki and Lanyi 1986).

Dynamic aspects of iron binding sites

Purple membranes with ^{57}Fe open a new possibility for investigating dynamics of a membrane bound protein in its interaction with the surrounding lipids. In the temperature range below 200 K solid state vibrations dominate the dynamics (Nienhaus et al. 1989). Mainly acoustic modes, involving collective motions of more than one bR molecule, determine the $\langle x^2 \rangle$-values. As seen from Fig. 6 the hydrated membrane is inhomogeneous with respect to solid state vibrations: the interface betweeen the membrane and bulk water as labelled by Fe^{2+} is less rigid ($\theta_D = 165$ K to 145 K) than the polar head groups of the lipids or the specific binding sites at the membrane where Fe^{3+} binds ($\theta_D = 200$ K to 230 K). The Debye temperatures can be compared with $\theta_D = 195$ K obtained in crystals of deoxymyoglobin (Parak et al. 1987). At lower pH values the rigidity of the membrane increases. This is in agreement with the finding that in lipid bilayers an ionisation loosens the structure because of electrostatic repulsion (compare for instance Hauser (1975)).

Dehydration makes the membrane homogeneous with respect to vibrations marked by ^{57}Fe. Below 200 K the Debye temperature is about 165 K at the Fe^{2+} and the Fe^{3+} position. Note that in this temperature region the dry membrane is less rigid than the hydrated mem-

brane. This is, however, only valid with respect to the solid state vibrations. At temperatures about 200 K hydration increases segmental motions as seen from the increase of the $\langle x^2 \rangle$-values.

Functional properties of iron binding sites

The Mössbauer-spectroscopic data indicated that Fe^{2+} is confined to the interface between the surface of the membrane and the bulk-phase. On the other hand, Fe^{3+} cations are directly liganded to the lipid- and/or protein moiety of purple membrane. In the following paragraph the functional nature and the location of these sites will be further discussed.

An indication that defined sites may exist is the observed retardation of the photocycle by Fe^{3+} and partly Cr^{3+} in a concentration range of three to five cations per bR. This stoichiometry suggests that at least three ferric ions are responsible for this effect. A possible explanation might be found in the special chemistry of trivalent iron and chromium. Under non-aqueous conditions both cations form trinuclear clusters with six acetate molecules (Figgis and Robertson 1965). It is tempting to speculate that at the membrane surface Fe^{3+} (or Cr^{3+}) aggregate to form similar complexes. Indeed, the Mössbauer experiments at low temperatures showed that at higher concentrations of iron the Fe-atoms are spin-spin coupled. This indicates a close spatial connection of the metal ions leading to a high additional positive charge on a restricted area of the purple membrane surface.

The question arises as to where this area might be located. As already mentioned it is not possible from these Mössbauer experiments to distinguish between lipid- and/or protein binding sites. However, preliminary data from Mössbauer measurements on purple membranes in which the native lipids were exchanged against detergents indicated that Fe^{3+}-binding sites still exist provided that the delipidation was complete. In these experiments Fe^{3+}-bR was solubilized by Triton X-100 and the native lipids were substituted by deoxycholate (DOC) according to the method of Huang et al. (1980). The Mössbauer spectra of the Triton-treated membrane as well as the DOC-membrane were similar to the native purple membrane. In further experiments using solid state NMR spectroscopy on bR labeled with (4-^{13}C)-Asp (Engelhard et al. 1989a) it could be shown that lanthanide shift reagents such as Eu^{3+} or Pr^{3+} interact with side chain carboxyl-groups of Asp residues (Engelhard et al., unpublished result). In another series of experiments the X-ray diffraction pattern of Fe^{3+} treated bR demonstrated that the interaction of Fe^{3+} with the purple membrane disturbs the protein lattice (G. Büldt et al., personal communication). All these results provide evidence that the binding site of Fe^{3+} can be located on the protein part of the purple membrane. However, it should be noted that additional experiments using Mössbauer and solid state NMR spectroscopy are needed to unequivocally establish the Fe^{3+} binding-site.

A cation binding site of bR has already been identified for the trivalent cobalt complex $[Co(NH_3)_5H_2O]^{3+}$ which could be firmly attached to bacterioopsin by activating the photocycle (Engelhard et al. 1989b). The resulting $[Co(NH_3)_5$-protein]-complex was impaired in function, structure, and chromophore-protein interaction. Because the Co-protein linkage was stable enough to withstand the conditions of protein chemistry two Co-containing peptides could be isolated and sequenced. The peptides stem from the C-terminal and the loop region of helices C and D and confined either two Asp (^{102}Asp-Ala-Asp) or two Glu (^{232}Glu-Ala-Glu).

These sequences might also be ligands for Fe^{3+} binding. If this assumption is correct than the positive charges of the three Fe^{3+} ions would be on the cytoplasmic membrane surface right above two internal aspartic acids (Asp85 and Asp96). It has already been shown that internal Asp residues are undergoing protonation-deprotonation reaction during the photocycle (Engelhard et al. 1985; Eisenstein et al. 1987). Site specific mutation of Asp85 and Asp96 had a dramatic effect on chromophore and proton pump (Mogi et al. 1988; Butt et al. 1989). In these experiments, it was demonstrated that the replacement of Asp96 by Gly or Asn reduces the photocycle turnover by two orders of magnitude. The inhibited step of the reaction cycle is, similar to the Fe-bR samples, the M-decay, i.e. the reprotonation of the Schiff base. It was concluded that Asp96 is an essential member of the proton uptake path (Butt et al. 1989; Tittor et al. 1989; Gerwert et al. 1989; Stern et al. 1989).

If one assumes that the peptide ^{102}Asp-Ala-Asp of the Co-binding site, which is only six residues away from Asp96, binds the Fe^{3+}-cations then this site might be part of the proton sink on the cytoplasmic surface. One can then imagine that a cluster of positive charges at this position might impede the funneling of a proton to the proton transfer chain. In conclusion, an area close to Asp102 and Asp104 or involving these two amino acids might include the site where the proton is taken up from the cytoplasmic medium.

Acknowledgements. This work was supported by the Deutsche Forschungsgemeinschaft and by the Fonds der Chemischen Industrie. We thank W. Stoeckenius for critically reading the manuscript and R. Müller, J. Püttmann-Wunderlich and A. Scholz for excellent technical help. The atomic absorption measurement by R. Alt and B. Messerschmidt is greatfully acknowledged.

References

Ariki M, Lanyi JK (1986) Characterization of metal ion-binding sites in bacteriorhodopsin. J Biol Chem 261:8167–8174

Ariki M, Madge D, Lanyi JK (1987) Metal ion binding sites of bacteriorhodopsin: Laser-induced lanthanide luminescence study. J Biol Chem 262:4947–4951

Bjerrum J, Schwarzenbach G, Sillen LG (1958) Stability constants of metal-ion complexes, Part I and II. The Chemical Society, London

Butt H-J, Fendler K, Bamberg E, Tittor J, Oesterhelt D (1989) Aspartic acids 96 and 85 play a central role in the function of bacteriorhodopsin as a proton pump. EMBO J 8:1657–1663

Chang CH, Chen JG, Govindjee R, Ebrey T (1985) Cation binding by bacteriorhodopsin. Proc Natl Acad Sci USA 82:396–400

Chang CH, Jonas R, Melchiore S, Govindjee R, Ebrey TG (1986) Mechanism and role of divalent cation binding of bacteriorhodopsin. Biophys J 49:731–739

Chronister EL, Corcoran TC, Song L, EL-Sayed MA (1986) On the molecular mechanisms of the Schiff base deprotonation during

the bacteriorhodopsin photocycle. Proc Natl Acad Sci USA 83:8580–8584

Corcoran TC, Ismail KZ, El-Sayed MA (1987) Evidence for the involvment of more than one metal cation in the Schiff base deprotonation process during the photocycle of bacteriorhodopsin. Proc Natl Acad Sci USA 84:4094–4098

Dér A, Tóth-Boconádi R, Keszthelyi L (1989) Bacteriorhodopsin as a possible chloride pump. FEBS Lett 259:24–26

Drachev AL, Kaulen AD, Skulachev VP (1978) Time resolution of the intermediate steps in the bacteriorhodopsin-linked electrogenesis. FEBS Lett 87:161–167

Drachev AL, Drachev LA, Kaulen AD, Khitrina LV (1984) The action of lanthanum ions and formaldehyde on the proton-pumping function of bacteriorhodopsin. Eur J Biochem 138:349–356

Duñach M, Seigneuret M, Rigaud J-L, Padros E (1987) Characterization of the cation binding sites of the purple membrane. Electron spin resonance and flash photolysis studies. Biochemistry 26:1179–1186

Duñach M, Seigneuret M, Rigaud J-L, Padros E (1988) Influence of cations on the blue to purple transition of bacteriorhodopsin. J Biol Chem 263:17378–17384

Duñach M, Padrós E, Muga A, Arrondo JLR (1989) Fourier-transform infrared studies on cation binding to native and modified purple membranes. Biochemistry 28:8940–8945

Edgerton ME, Moore TA, Greenwood C (1980) Investigation into the effect of acid on the spectral and kinetic properties of purple membrane from Halobacterium halobium. Biochem J 189:413–420

Eisenstein L, Lin SL, Dollinger G, Odashima K, Ding WD, Nakanishi K (1987) FTIR-difference studies on apoproteins. Protonation states of aspartic and glutamic acid residues during the photocycle of bacteriorhodopsin. J Am Chem Soc 109:6860–6862

Engelhard M, Gerwert K, Hess B, Kreutz W, Siebert F (1985) Light-driven protonation changes of internal aspartic acids of bacteriorhodopsin: An investigation by static and time-resolved infrared difference spectroscopy using [4-^{13}C] aspartic acid labeled purple membrane. Biochemistry 24:400–407

Engelhard M, Hess B, Chance M, Chance B (1987) X-ray absorption studies on bacteriorhodopsin. FEBS Lett 222:275–278

Engelhard M, Hess B, Emeis D, Metz G, Kreutz W, Siebert F (1989 a) Magic angle sample spinning ^{13}C nuclear magnetic resonance of isotopically labeled bacteriorhodopsin. Biochemistry 28:3967–3975

Engelhard M, Pevec B, Hess B (1989 b) Modification of two peptides of bacteriorhodopsin with a pentaaminecobalt (III) complex. Biochemistry 28:5432–5438

Figgis BN, Robertson GB (1965) Crystal-molecular structure and magnetic properties of $Cr_3(CH_3COO)_6OCl * 5H_2O$. Nature 205:694–695

Fischer U, Oesterhelt D (1979) Chromophore equilibria in bacteriorhodopsin. Biophys J 28:211–230

Gerwert K, Hess B, Soppa J, Oesterhelt D (1989) Role of aspartate-96 in proton translocation by bacteriorhodopsin. Proc Natl Acad Sci USA 86:4943–4947

Hauser H (1975) Lipids. In: Francks F (ed) Water. Plenum Press, New York, pp 209–303

Huang KS, Bayley H, Khorana HG (1980) Delipidation of bacteriorhodopsin and reconstitution with exogenous lipids. Proc Natl Acad Sci USA 77:323–327

Katre NV, Kimura Y, Stroud RM (1986) Cation binding sites on the projected structure of bacteriorhodopsin. Biophys J 50:277–284

Kimura Y, Ikegami A, Stoeckenius W (1984) Salt and pH-dependent changes of the purple membrane absorption spectrum. Photochem Photobiol 40:641–646

Kobayashi T, Othani H, Iwai J-I, Ikegami A, Uchiki H (1983) Effect of pH on the photoreaction cycles of bacteriorhodopsin. FEBS Lett 162:197–200

Maurer R, Vogel J, Schneider S (1987) Analysis of flash photolysis data by a global fit with multi-exponentials. I. Determination of the minimal number of intermediates in the photocycle of bacteriorhodopsin by the 'stability criterion'. Photochem Phobiol 46:247–253

Mogi T, Stern LJ, Marti T, Chao BH, Khorana HG (1988) Aspartic acid substitutions affect proton translocation by bacteriorhodopsin. Proc Natl Acad Sci USA 85:4148–4152

Mowery PC, Lozier RH, Chae Q, Tseng YW, Tayler M, Stoeckenius W (1979) Effect of acid pH on the absorption spectra and photoreactions of bacteriorhodopsin. Biochemistry 18:4100–4107

Nagle JF, Parodi LA, Lozier RH (1982) Procedere for testing kinetic models of the photocycle of bacteriorhodopsin. Biophys J 38:161–174

Nienhaus GU, Heinzl J, Huenges E, Parak F (1989) Protein crystal dynamics studied by time-resolved analysis of X-ray diffuse scaterring. Nature 338:665–666

Nozik AJ, Kaplan M (1967) Mössbauer resonance studies of ferrous ions in ice. J Chem Phys 47:2960–2977

Nozik AJ, Kaplan M (1968) Paramagnetic and electric quadrupole hyperfine interactions of ferric ions in ice and $FeCl_36H_2O$. J Chem Phys 49:4141–4149

Oesterhelt D, Stoeckenius W (1971) Rhodopsin-like protein from the purple membrane of Halobacterium halobium. Nature 233:149–152

Oesterhelt D, Stoeckenius W (1974) Isolation of the cell membrane of Halobacterium halobium and its fractionation into red and purple membrane. Methods Enzymol 31A:667–678

Oesterhelt D, Tittor J (1989) Two pumps, one principle: light driven ion transport in halobacteria. Trends Biochem Sci 14:57–61

Ohtani H, Kobayashi T, Iwai J-I, Ikegami A (1986) Picosecond and nanosecond spectroscopies of the photochemical cycles of acidified bacteriorhodopsin. Biochemistry 25:3356–3363

Ovchinnikov YA, Abdualev NG, Modyanov NN (1982) Structural basis of proton-translocating protein function. Ann Rev Biophys Bioeng 11:445–463

Parak F, Reinisch L (1986) Mössbauer effect in the study of structure dynamics. Methods Enzymol 131:568–607

Parak F, Finck P, Kucheida D, Mössbauer RL (1981) Fluctuations between conformational substates in deoxygenated myoglobin. Hyperfine Interact 10:1075–1078

Parak F, Knapp EW, Kucheida D (1982) Protein dynamics. Mössbauer spectroscopy on deoxymyoglobin crystals. J Mol Biol 161:177–194

Parak F, Hartmann H, Aumann KD, Reuscher H, Rennekamp G, Bartunik H, Steigemann W (1987) Low temperature X-ray investigation of structural distribution in myoglobin. Eur Biophys J 15:237–249

Singh GP, Parak F, Hunklinger S, Dransfeld K (1981) Role of adsorbed water in the dynamics of metmyoglobin. Phys Rev Lett 47:685–688

Stern LJ, Ahl PL, Marti T, Mogi T, Duñach M, Berkowitz S, Rothschild KJ, Khorana HG (1989) Substitution of membrane-embedded aspartic acids in bacteriorhodopsin causes changes in different steps of the photochemical cycle. Biochemistry 28:10035–10042

Sternheimer RM (1963) Quadrupole antishielding factors of iron. Phys Rev 130:1423–1425

Stoeckenius W, Bogomolni RA (1982) Bacteriorhodospin and related pigments of halobacteria. Ann Rev Biochem 52:567–615

Szundi I, Stoeckenius W (1987) Effect of lipid surface charges on the purple-to-blue transition of bacteriorhodopsin. Proc Natl Acad Sci USA 84:3681–3684

Szundi I, Stoeckenius W (1989) Surface pH controls purple-to-blue transition of bacteriorhodopsin. A theoretical model of purple membrane surface. Biophys J 56:369–383

Tittor J, Soell C, Oesterhelt D, Butt H-J, Bamberg E (1989) A defective proton pump, point-mutated bacteriorhodopsin Asp96→Asn is fully reactivated by azide. EMBO J 8:3477–3482

Váró G, Lanyi JK (1989) Photoreactions of bacteriorhodopsin at acid pH. Biophys J 56:1143–1151

Zubov B, Tsuji K, Hess B (1986) Transition kinetics of the conversion of blue to purple bacteriorhodopsin upon magnesium binding. FEBS Lett 200:226–230